Investigation of heat transfer in wavy and dual wavy micro-channel heat sink using alumina nanoparticles

Case Studies in Thermal Engineering 28 (2021) 101515

Contents lists available at ScienceDirect

Case Studies in Thermal Engineering

journal homepage: www.elsevier.com/locate/csite

Investigation of heat transfer in wavy and dual wavy micro-channel heat sink using alumina nanoparticles

Muhammad Zia Ullah Khan [a], M. Yamin Younis [b], Naveed Akram [b,g,**], Bilal Akbar [b], Umair Ahmed Rajput [c], Rumeel Ahmad Bhutta [d], Emad Uddin [e], Muhammad Ahsan Jamil [e], Fausto Pedro García Márquez [f,*], Fahad Bin Zahid [g]

[a] COMSATS University Islamabad, Sahiwal, Pakistan
[b] Department of Mechanical Engineering, Mirpur University of Science and Technology (MUST), Mirpur, 10250, AJK, Pakistan
[c] Mechanical Engineering Department, QUEST, Nawabshah, 67450, Pakistan
[d] Ulster University, United Kingdom
[e] Department of Mechanical Engineering, School of Mechanical and Manufacturing Engineering (SMME), National University of Science and Technology, Islamabad, Pakistan
[f] Ingenium Research Group, University of Castilla-La Mancha, F.P.G.M, Spain
[g] Department of Mechanical Engineering, Faculty of Engineering, University of Malaya, Kuala Lumpur, 50603, Malaysia

HIGHLIGHTS

- The effect of geometry and nanoparticles concentrations on the heat transfer and friction factor of the microchannel.
- The conventional straight channel is compared with uniform wavy, dual wavy channel considering the equal volume.
- The optimum channel is identified by using the Thermal Performance Factor considering the effect of heat transfer and pressure drop.
- The heat transfer performance of all wavy channels was more than double compared to straight channel and increased with an increase in Reynolds number.
- The base wall temperature reduced on average from 6 °C to 10 °C for a 100 to 900 increase in Reynolds number compared to the straight channel.

ARTICLE INFO

Keywords:
Nanofluids
CFD
Secondary vortices
Microchannels
Heat transfer

ABSTRACT

Thermal management is crucial for the proper functioning of a system whether it is in electronics, process industry, automobile, and renewable devices. Micro-channel heat exchanger has proved to be efficient in heat ejection from renewable systems due to high heat transfer surface to volume ratio. This study focuses on evaluating the cooling performance of straight, wavy, and dual wavy Micro-Channel Heat Exchanger by modelling the heat transfer model in ANSYS Fluent. The incompressible fluid is considered in the laminar regime using alumina-based nanofluids with 1%, 3%, and 6% concentration. The solution is computed by selecting SIMPLE pressure-velocity coupling scheme with second-order momentum and energy discretization. Nusselt number, pressure drop, base temperature, and Thermal Performance Factor (TPF) are used as performance parameters for comparing nanofluids performance at Reynolds number range of 100–900. For straight, wavy, and dual wavy model heat transfer, as well as pressure drop, increased with Reynolds number. It is observed that wavy and dual wavy channels compared to straight channel

* Corresponding author.
** Corresponding author. Department of Mechanical Engineering, Mirpur University of Science and Technology (MUST), Mirpur, 10250, AJK, Pakistan.
E-mail addresses: naveed.me@must.edu.pk (N. Akram), FaustoPedro.Garcia@uclm.es (F.P. García Márquez).

https://doi.org/10.1016/j.csite.2021.101515
Received 27 October 2020; Received in revised form 13 September 2021; Accepted 27 September 2021
Available online 29 September 2021

improved convective heat transfer due to the formation of secondary vortices at the curved section. Dual wavy with wavy base and flat base wall showed highest Nusselt number increase of more than double when compared with straight channel of equal concentration. For 6% nano particles addition in all channels, on average both dual wavy channels showed highest improvement of 8% when compared with 0% concentration channel. Dual wavy channel with a flat base and wavy base reduced the base heater temperature by 10 °C and 9 °C compared to the straight channel. A maximum Thermal Performance Factor of 2.2 is achieved for dual wavy channel with a wavy base configuration with 6% nanoparticles.

Nomenclature

Symbol

L (μm)	Overall length of channel
H (μm)	Height of the channel
W (μm)	Width of the channel
P (μm)	Distance between two crest (Top)
b (μm)	Distance between two crest (Side)
a (μm)	Wave amplitude
$\mathbf{D_h}$ (mm)	Hydraulic diameter of channel
ρ (kg/m^3)	Density
$\boldsymbol{\mu}$ (Pa.s)	Viscosity
$\boldsymbol{C_p}$ (J/kg.K)	Specific Heat
k(W/m.K)	Thermal Conductivity
h(W/m^{2}K)	Convective heat transfer coefficient
ΔP	(Pa) Pressure Drop
T(K)	Temperature
U(m/s)	Velocity of fluid
Q (W/m^2)	Heat flux

Symbol

f	Friction Factor
Re	Reynolds Number
Nu	Nusselt Number
TPF	Thermal Performance Factor
$\boldsymbol{\delta}$	Nanoparticles concentration

Subscript

f	Fluid
nf	Nanofluid
bf	Base Fluid (Water)
s	Solid
o	Straight channel property
out	Outlet
in	Inlet
w	Wall
avg	Average

1. Introduction

The power consumption of electronic components and subsequent performance levels are achieved by effective heat removal from e-chips. By current practice, air cooled heat sinks are widely used [1,2]. With each passing decade, the size of electronic chips has reduced significantly with increased performance efficiency and as a result, high thermal flux is released. Air with low thermal conductivity and heat capacity in not efficient for increased thermal flux [3]. This lead to the integration of fluid cooled heat sinks in electronic systems [4–7]. Liquids with better thermal characteristics than air such as water become standards for most cooling applications. The performance factor of such liquid cooled heat sink is dependent on heat sink physical configuration such as the shape of the heat sink and the type of fluid used for removal of thermal heat from the sink.

In term of physical configuration, the introduction of microchannels embedded into the heat sinks have been studied by several

researchers with positive results [8–12]. It has wide applications related to heat transfer in refrigeration and air conditioning, microelectronics, biomedical, solar panel, aerospace, and process industry. The geometry of the micro-channel system itself has been investigated with variable shape configurations such as tree-shaped [13], fractal shaped [14] and hybrid structures [15]. These shape deviation from convectional straight microchannels have been shown to enhance the heat transfer capabilities with promising results in the wavy (sinusoidal) channels [16,17]. Sui et al. [16] tested 60–62 wavy microchannels of copper concluding high heat transfer performance and justified that pressure drop in wavy channel compared to heat transfer is an affordable trade off.

Physical configuration aside, the type of cooling liquid used in these micro channels affects the performance of heat sinks. Techniques have been employed to improve thermal performance by utilizing phase-change materials [18–20] and nano-fluids [21–24]. Since the introduction of nano-fluids, it is argued that higher thermal conductance of nano-sized solid particles mixed with a thermal convective liquid, such as water, would improve the overall thermal convective performance of the cooling liquid in a heat sink [25].

In recent studies, the effect of nanoparticles such as graphite for industrial microchannel with a volume fraction (ϕ) of 0.5–2% in a distilled water as base liquid showed a positive correlation with convective heat transfer (h) rate, an increase in nano-particle increased convection rate by 15–25% [26]. Similarly, with a silver (Ag)-water nano-fluid increased performance was reported as compared to base fluids, and it is shown that heat sinks with frequent path changes are more effective, but the results of this study were inclusive [27]. In terms of the effect of nano-particles on sinusoidal mini-tube, a detailed study is performed by Liu et al. [28]. They observed heat transfer and convection rate of silicon-carbide (SiC) nano-fluid, with a volume fraction (ϕ) of 4% and particle diameter (d) ranging from 16 to 90 nm in a base fluid of ethyle-glycol/water (50:50) mixture. It is seen from their data that nanoparticles of SiC with d = 90 nm were most effective.

Researchers have studied nano additives for performance enhancement of shell and tube heat exchanger [29], car radiator [30], double tube counter flow heat exchanger [31,32], photovoltaic thermal system [33] and solar air heater [34–36]. It must be noted here that the addition of nano-additives in a base liquid increases the viscosity of base liquid, and the leniency towards Newtonian or non-Newtonian would depend on exposed temperature [23]. In case of aluminium oxide (Al_2O_3) nano-additive, with 1–10% concentration and base liquid of ethylene glycol-water mixer, the nano-fluid behaved has Newtonian fluid under temperature ranges of 0 °C to 90 °C, and as non-Newtonian between −35 °C to 0 °C [37]. In case of nano additives of silicon dioxide (SiO_2) in ethylene glycol-water mixer, Newtonian behaviour was absent in temperature ranges of −35 °C to 50 °C when the volume fraction of additive is 0%–6% [37–39]. Numerical simulation for convective heat transfer estimation by introduction of nano-particles like Al_2O_3 [40–47], CuO [40,43,46,48,49], SiO_2 [46], Cu [50,51], ZrO2 [44], TiO2 [45] and ZnO [46] in different shapes channel like simple straight [44,45], with vortex generators [43], with Trapezoidal rib-groove [46] and triangular enclosure [51] are studied. Effect of nanoparticles on uncommon geometries like wavy [52], curvy [53], and zigzag [53] configurations have sufficient area to work.

For the current study, the performance of wavy and dual wavy microchannel is numerically investigated to gauge their performance level subjected to 1%, 3% and 6% nano-fluid concentration of aluminium oxide (Al_2O_3). The base liquid is de-ionized water with temperature dependent thermophysical properties. For comparison purpose of the straight, wavy, and dual wavy channel, overall volume of the geometric models is kept the same. The fully developed flow is introduced in the channels to maintain the same flow entrance conditions. The amplitude of the wave is selected between an optimum range of 0.06–0.22, proposed for best thermal performance [52].

The paper is presented as follows: Section II presents the methodology, including the geometry, mesh, governing equations, setup, and boundary conditions parametric definition and validation and test matrix; Section III shows the main results and discussion, including the effect of nano-particles and geometry on the base temperature, the effect of nano-particles on thermal performance factor and the effect of channel geometry with nano-particles.; Finally, the paper concludes with Section IV, where the main conclusions are presented. The studied design can serve as a substitute in microchannel base heat transfer applications related to solar panel cooling [54,55], gas turbine blade [56], and combustor cooling [57], and microelectronic cooling [58,59].

2. Methodology

2.1. Geometry

A geometry of straight and wavy microchannel is developed using SolidWorks software. Quantitative geometrical attributes are represented in Table 1 where H_d is hydraulic diameter, W is width, L is length, a is amplitude, P is the pitch of wavy channel and b is pitch of dual wavy base. The overall volume of all channels is fixed for performance comparison purposes. The channels with Straight, wavy, dual wavy with flat base (FB), and dual wavy with wavy base (WB) are studied, three channels will have equal heated area and one will have more heated area. Aspect ratio, length, and amplitude 'a' are fixed by referring from the research study of Mohammad et al. [52], together with the selection channel with optimum overall thermal performance.

Table 1
Parameters of channel.

Dimensions of Microchannels					b (μm)
H_d (μm)	W (μm)	L (μm)	a (μm)	P (μm)	
335.19	280	10,916	375	2000	3158

2.2. Mesh

The meshing of the microchannel models is performed in ANSYS Meshing module by using tetrahedral element type (see Fig. 2c). The grid independence is shown in graphical and error representation in Fig. 2a and Table 2. It is achieved at 4,132,128 number of elements with average mesh orthogonality, skewness, and aspect ratio of 0.814, 0.124, and 8.05. Grid independence is achieved by varying mesh size from coarse to finer mesh.

2.3. Governing equations

The fluid flow and heat transfer are governed through continuity, momentum and energy equations (1)–(3) [43,60].

$$\nabla.U = 0 \tag{1}$$

$$U.\nabla(\rho U) = -\nabla p + \nabla.(\mu.\nabla U) \tag{2}$$

$$U.\nabla\left(\rho C_p T_f\right) = \nabla.\left(k_f \nabla T_f\right) \tag{3}$$

In the governing equations: ρ is the density of the fluid; U is the velocity; μ represents viscosity; k is the thermal conductivity; T represents temperature, and; C_p is specific heat.

2.4. Setup and boundary conditions

Numerical analysis is performed using Fluent module of ANSYS 19.2. The incompressible fluid is considered with temperature dependent properties. They are introduced in piecewise polynomial for both De-ionized water [61,62] and nanofluids [63]. Thermophysical properties of the base fluid and nanoparticles are shown in Table 3. Fully developed flow profile is imported in the channel by performing additional simulations for each particle concentration. Heat flux condition with the value of 200,000 W/m^2 is applied in the bottom wall of the straight, wavy, and dual wavy. Top and side walls are set as adiabatic in Fig. 3a, b, 3c, and 3d model. The temperature of the inlet fluid is set to 298K. For modelling heat transfer, thin wall model approach (no axial wall conduction) is applied at the side walls due its good approximation with experimental results for single channel [64] and also reduced mesh size, and Aluminum is set as a solid substrate with 250 μm side wall thickness and 1000 μm base wall thickness [64]. Eulerian approach is used for modelling Nanofluids in the channel [65]. SIMPLE algorithm is used for pressure velocity coupling with second order upwind schemes to compute solution numerically. Xeon 5650 dual hexa core processor with 60 GB Ram is utilized for computational approach. Average time for the completion of one simulation is 5 h.

2.5. Parametric definition

The results of the study are presented by using subsequent parameters. The Reynolds number (*Re*) depending on hydraulic diameter (D_h) of channel and fluid properties are given by equations (5) and (6), respectively,

$$Re = \frac{\rho u_{in} D_h}{\mu} \tag{5}$$

$$D_h = \frac{2WH}{W+H} \tag{6}$$

where: W is the width and H the height of the microchannel; μ represents the viscosity, and; u_{in} is the velocity of the fluid.

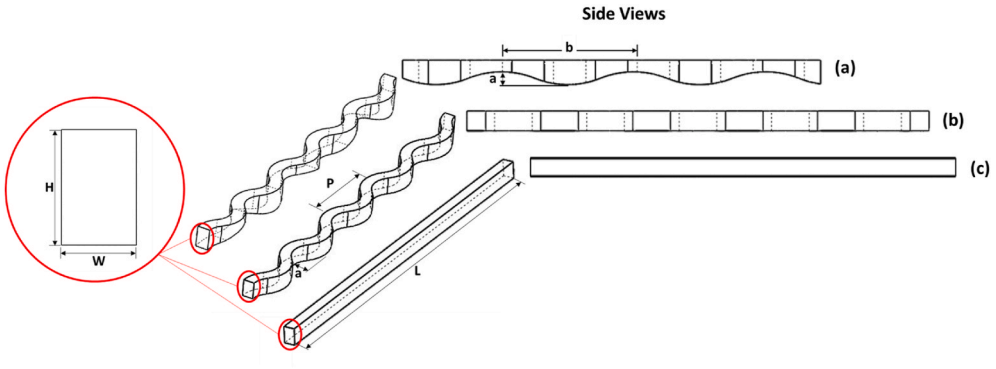

Fig. 1. Geometry a) Dual wavy, b) Wavy, and c) Straight.

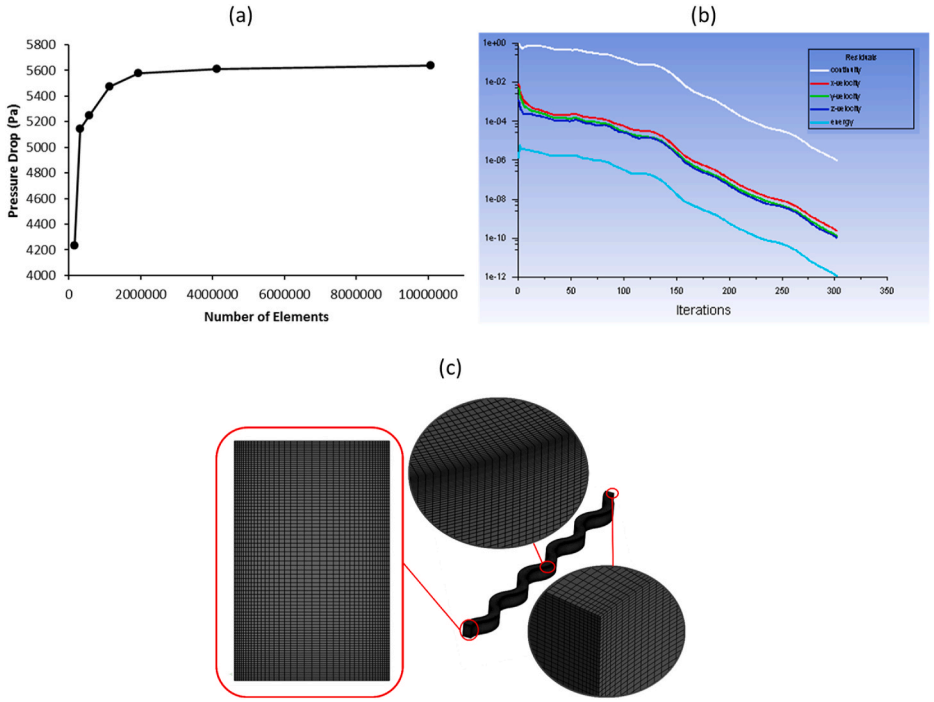

Fig. 2. (a)Grid Independence for model, (b) residuals and (c) meshed model.

Table 2
Grid Independence study.

Sr. no	Number of Elements	Pressure Drop (Pa)	% Difference
1	171,601	4234	–
2	325,420	5142	21.4%
3	565,110	5248.03	2.1%
4	1,141,504	5471.87	4.3%
5	1,929,792	5575.11	1.9%
6	4,132,128	5612.32	0.7%
7	10,066,875	5640.26	0.5%

Table 3
Properties of pure water and alumina.

	Al_2O_3 [63]	Pure-Water [61,62]
μ (Pa.s)		$2.761 \times 10^{-6} \exp\left(\frac{1713}{T}\right)$
$\boldsymbol{k}$ (W/m.K)	36	$0.6 + 2.5 \times 10^{-5} T$
$\boldsymbol{C_P}$ (J/kg.K)	765	4180
ρ (kg/m^3)	3970	1000

Properties of alumina and base fluid at different nanoparticles concentrations (σ) is modelled using nanofluids expressions for density ρ_{nf}, viscosity μ_{nf}, specific heat $C_{p,np}$ and thermal conductivity k_{nf}, given by equations 7–10 [2,43,51].

$$\rho_{nf} = (1-\delta) + \delta\rho_s \tag{7}$$

$$\left(\rho C_p\right)_{nf} = (1-\delta)\left(\rho C_p\right)_f + \delta\left(\rho C_p\right)_s \tag{8}$$

$$\mu_{nf} = \frac{\mu_f}{(1-\delta)^{2.5}} \tag{9}$$

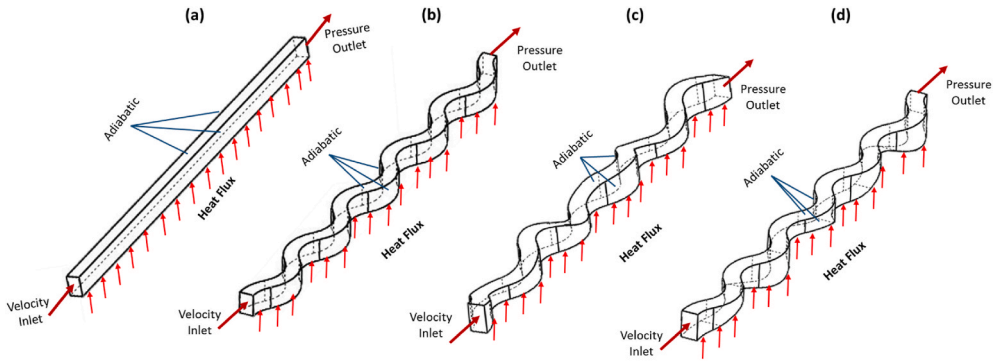

Fig. 3. Boundary Conditions a) Straight channel, b) Wavy channel, c) Dual wavy with Flat Base (FB), and d) Dual wavy channel with Wavy Base (WB).

$$\frac{k_{nf}}{k_f} = \frac{k_s + 2k_f - 2\delta(k_f - k_s)}{k_s + 2k_f + \delta(k_f - k_s)} \tag{10}$$

For evaluating the convective heat transfer, the Nusselt number (*Nu*) is calculated by equation (11).

$$Nu = \frac{h.D_h}{k_{f,avg}} \tag{11}$$

where

$$h = \frac{Q}{T_w - \frac{T_{in}+T_{out}}{2}} \tag{12}$$

In equations 11 and 12: h is the heat transfer coefficient; Q is the heat flux, and; k_{bf} is average base fluid thermal conductivity. The apparent friction factor (*f*) of the overall microchannel is expressed by equation (13)

$$f = \frac{(\Delta P/L)D_h}{2\rho u_{in}^2} \tag{13}$$

where

$$\Delta P = P_{out} - P_{in} \tag{14}$$

For addressing the overall performance of wavy and dual wavy microchannel, a performance comparison with conventional straight microchannel is made using Thermal Performance Factor (TPF) [2,43].

$$TPF = \frac{(Nu/Nu_0)}{(f/f_0)^{1/3}} \tag{15}$$

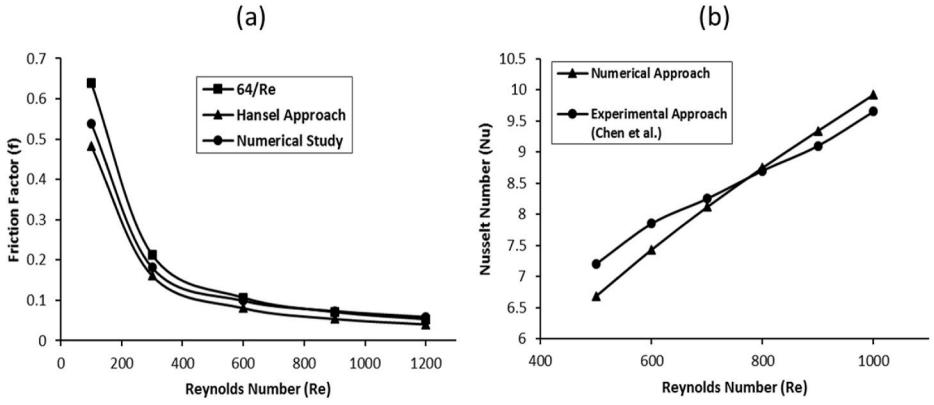

Fig. 4. Validation of Numerical Model a) For friction factor with Hansel et al. [66], b) For Nusselt number with (H = 100 μm, W = 400 μm) Chen et al. [67].

where Nu_o and f_0 represents Nusselt number and friction factor of benchmark channel, where in this case is the straight channel. A value of TPF greater than 1 will represent studied channel superior in heat transfer than benchmark channel.

2.6. Validation and test matrix

Validation of Nusselt number and friction factor is performed with the study of Hansel et al. [66] and Chen et al. [67] for verifying the performance prediction capability of the numerical model. The numerical model developed considering same geometry, flow and boundary conditions of experimental study, fairly validates with the experimental model with an average error of approximately 3%. The error can be due to uncertainties during experimentation which are limited in numerical modelling. (Fig. 4).

Test matrix for the overall study is presented in Table 4 where 41 models are run for fully developed profile extraction which are exported to simulate 50 models.

3. Result and discussion

3.1. Effect of nano-particles and geometry on the base temperature

Base cooling with variation in Reynolds number and particles concentration for straight and wavy microchannel can be seen in Fig. 5a and b. For all, four cases, cooling effect on the base is high in case of the dual wavy channel with wavy base, straight channel, on the other hand, proved least favorable in cooling. It can also be observed that with the increment in Reynolds number more heat is extracted from the heating surface. So, the wavy and dual wavy channels can cool the heated surface more efficiently than straight. Considering Reynolds number with 0% concentration, a maximum temperature reduction of 8.5 °C is achieved at Re = 600 for wavy channel, dual wavy with wavy base provided 10.5 °C reduction at Re = 300, and dual wavy with flat base provided 9.8 °C reduction in temperature at Re = 300.

It can be seen in Fig. 6b that with the increase in nanoparticles concentration base temperature of the straight, wavy, and both dual wavy channel decreases, thus depicting enhancement in heat carrying capability of fluid. The highest cooling effect is produced by the dual wavy change due to high disturbance in the flow by the periodic variation of geometry path and the variation of cross-section due to wave in the base. High fluctuations of the flow and creation of backflow flow limited the laminar response to 600 Reynolds number for the dual wavy channel. This is due to the divergent section of the channel as can be seen from the side view of the dual channel in Fig. 1. Considering Reynolds number with 6% concentration, a maximum temperature reduction of 8.7 °C is achieved at Re = 600 for wavy channel, dual wavy with wavy base provided 9.7 °C reduction at Re = 300, and dual wavy with flat base provided 9.1 °C reduction in temperature at Re = 300.

The contours of base cooling in Fig. 6 depicts reduced temperature in the base for the wavy and dual wavy channel. The low temperature is due to mixing phenomena created by the vortices due to high and low velocity regions at the maximum wave amplitudes. The high temperature zones in dual wavy flat and wavy base channel are at different spots. For Re = 100, the lowest maximum hot spot of 329K is seen for dual wavy with wavy base. However, for Re = 600, the lowest maximum hot spot of 311K is seen for wavy channel in Fig. 6b but the dual wavy channel in Fig. 6c and d has more area with low temperature.

3.2. Effect of nano-particles on thermal performance factor (TPF) and Prandtl number (Pr)

The requirement of optimum heat exchanger involves low pressure drop and high Nusselt number. TPF is a non-dimensional parameter used for identifying the performance of microchannel by relation pressure drop and Nusselt number trade off of existing and improved channel. Fig. 7a, b, 7c, and 7d represent performance enhancement of straight, wavy, dual wavy flat base (FB) and wavy base (WB) channel with the addition of nanoparticles of different concentration by keeping base fluid as a benchmark. Fig. 7a shows that for concentrations TPF is greater than 1, showing that Nusselt number overtook the pressure drop. For low Reynolds number, 3% and 6% concentration fluid showed enhancement in heat transfer, but beyond Re = 300 pressure drops became dominant, showing reduction in TPF. Fig. 7b shows TPF variation with Reynolds number, which at low nanoparticles concentration, TPF remained nearly 1, and at high values above Re = 600, it increased due to the formation of vortices, see Fig. 7(b,e,f). For high concentration, TPF first decreases due to pressure drop dominance with increase in nanoparticles concentration and then increased to peaked at Re = 900. It is because of the development of reoccurring vortices in the wavy channel.

Performance of dual wavy channel is shown in Fig. 7c and d, representing an increase in performance with the addition of

Table 4
Test matric of numerical study.

	Model	No of cases
To Develop Flow	Straight Channel (0%,1%,3%,6%)	16
	Wavy Channel (0%,1%,3%,6%)	16
	Dual Wavy Channel (0%,3%,6%)	9
Developed Flow	Straight Channel (0%,1%,3%,6%)	16
	Wavy Channel (0%,1%,3%,6%)	16
	Dual Wavy Channel Flat Base (0%,3%,6%)	9
	Dual Wavy Channel Wavy Base (0%,3%,6%)	9

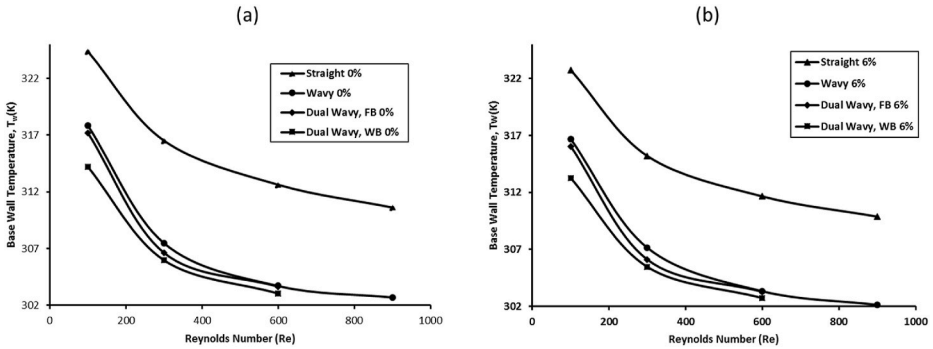

Fig. 5. Base wall temperature cooling with Reynolds number a) 0% nanoparticles b) 6% nanoparticles.

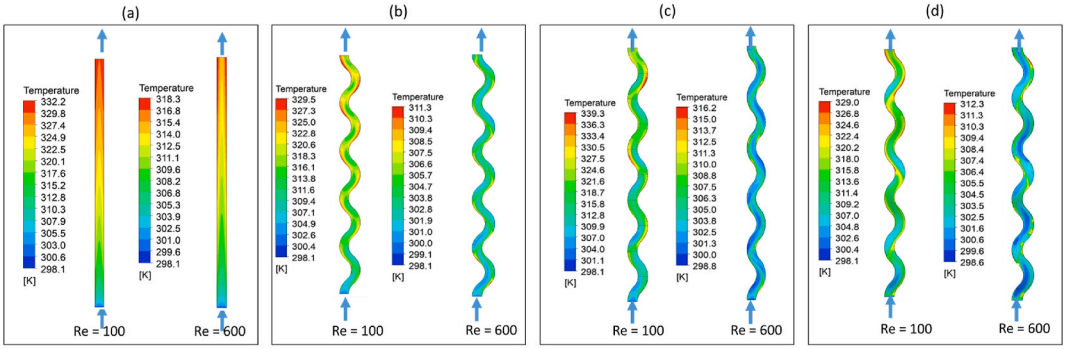

Fig. 6. Temperature contours on channel heated face a) Straight channel, b) Wavy channel, c) Dual wavy channel (FB), and Dual wavy channel (WB).

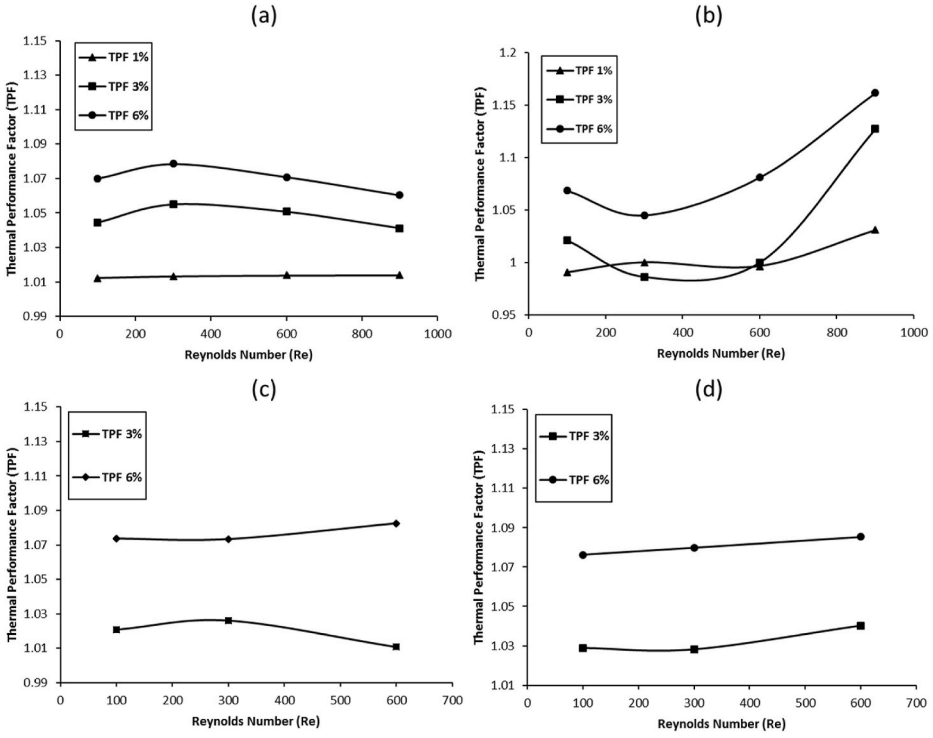

Fig. 7. TPF variation with Reynolds number for a) straight model, b) Wavy model, c) Dual wavy model (FB), and d) Dual wavy model (WB).

nanoparticles. A diverging section in Fig. 7b is due to increase in Nusselt number for 6% concentration with less increment in pressure drop. It can also be seen in Fig. 11 that depicts that intensity of heat transfer in some case increases high and in others low compared to the pressure drop. Fig. 8c and d shows that formation of regular vortices at the high aspect ratio cross section of the channel. The development of vortices begins at low Reynolds number, and its intensity became more with the increase in Re value.

Temperature variation in the cross section of the channel is shown in Fig. 9, where temperature behavior for a straight channel is uniform. However, Fig. 9b, c, and 9d constitute irregular contours depicting cooling effect produced due to heat extraction from the base by circulating flow. Furthermore, flow vortices periodic temperature contours on the cross section of dual wavy channel are visible in Fig. 9c and d, i.e., velocity and temperature dissipation phenomena.

The Prandtl number depends on thermal conductivity (k), viscosity (μ), and specific heat (C_p) of the fluid. In this study, fluid properties are temperature dependent as represented in Table 2. The Pr presented in Fig. 10 with Reynolds number for different geometries and nano-additive concentration, is evaluated on the temperature of the fluid at the channel outlet thus, as different geometries have different outlet fluid temperatures the respective Pr value is different as shown in Fig. 10. It can be observed that Prandtl number decreases with increment in particles concentrations because of enhancement of thermal diffusivity or thermal conductivity. On the other hand, it increases with Reynolds number depicting increment in momentum diffusivity. Based on geometry, wavy channel shows high momentum diffusivity, this is due to the formation of rotating vortices throughout the length of the channel compared to dual wavy channel which experience vortices only at bigger cross section.

3.3. *Effect of channel geometry with nano-particles*

Heat transfer coefficient, pressure drop, and TPF with Reynolds number, geometry, and nano-particles concentration variation are shown in Fig. 11. It can be noted that the introduction of nanoparticles improves the heat transfer coefficient, likewise, pressure drop also increases. Furthermore, change in geometry from straight to wavy and dual wavy provided enough improvement in heat transfer coefficient due to flow mixing and, for the same reason, requirement of pumping also increases due to pressure drop increment. Pressure drop for both dual wavy channels was approximately same but more than wavy and straight channel.

TPF estimation of the wavy and dual wavy channel by keeping a benchmark straight channel of respective particles concentration is given in Fig. 11c. It can be observed that, for all Reynolds numbers, TPF is greater than 1, showing positive response towards change in geometry due to the dominance of Nusselt number compared to pressure drop. For wavy channel, a decrease in slope is experienced above Re = 600, whereas both dual wavy channels suffer from reduced TPF slope after Re = 300. Furthermore, a uniform behavior of TPF is observed for the dual wavy case as compared to the erratic behavior of the wavy channel. The reason behind this trend is periodic vortices formation from the low to high Reynolds number for the dual wavy channel. Dual wavy with wavy base utilizes the vortices for heat dissipation but when heat flux is introduced at flat base the small vortices on the upper side of the channel as shown in

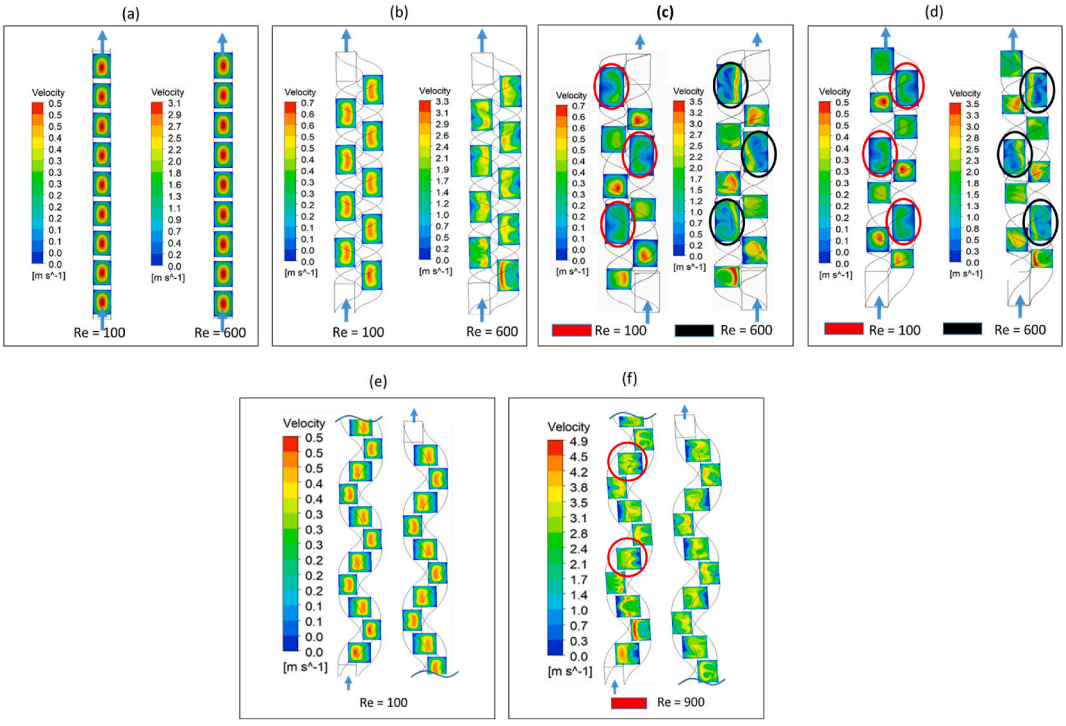

Fig. 8. Velocity Contours at cross-section with 6% Alumina a) Straight channel, b) Wavy channel, and c) Dual wavy channel (FB), and d) Dual wavy channel (WB), Velocity Contours at cross-section with 6% Alumina for Wavy channel at d) Re = 100 and e) Re = 900.

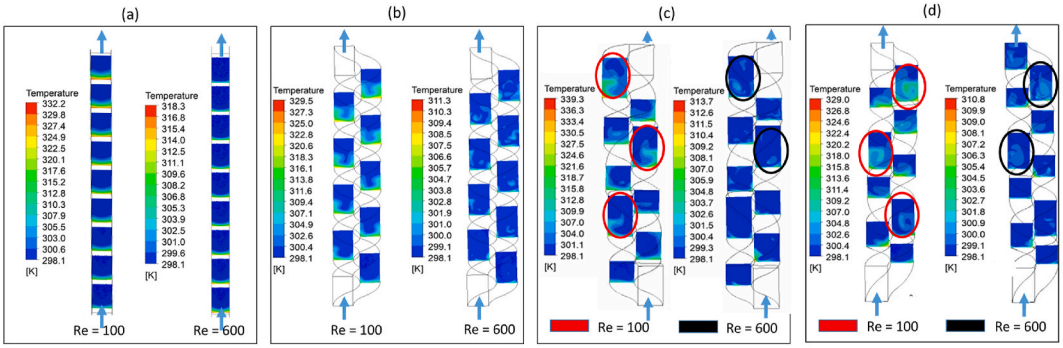

Fig. 9. Temperature Contours at cross-section with 6% Alumina a) Straight channel, b) Wavy channel, c) Dual wavy channel (BH), and d) Dual wavy channel (TH).

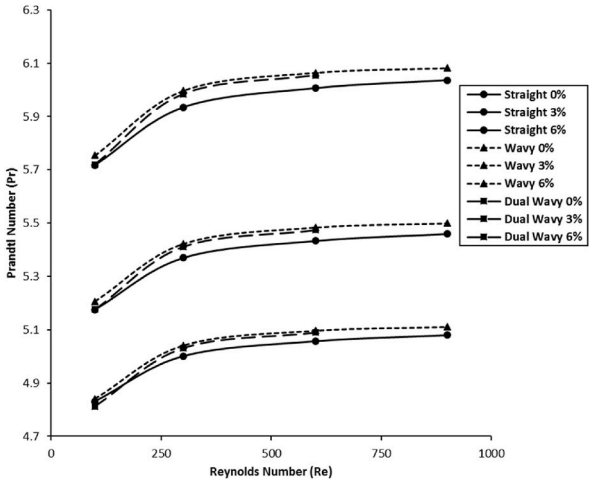

Fig. 10. Prandtl number (Pr) variation with Reynolds number.

Fig. 8c were unable to dissipate heat efficiently, thus both dual channels provided approximately equal pressure drop but top wall heated channel provided less convection. Therefore, for all Reynolds number, TPF of flat base dual wavy channel lagged, especially at Re = 600. A maximum TPF of 2.2 is seen for dual wavy channel with wavy base at Re = 600 at 6% particles concentration, conversely, flat base channel failed to show significant enhancement at the same velocity and concentration. Flat base channel performed better with approximately 14% at Re = 300 when compared with wavy but remained below wavy base channel.

4. Conclusions

The study investigated the effect of channel shape and inclusion of nanoparticles on the heat transfer performance with heat flux boundary conditions using numerical computation. Dual wavy with flat a base and wavy base showed highest Nusselt number increase of more than 50% when compared with straight channel of equal concentration. For 3% nano particles addition in all channels, on average straight channel showed the highest improvement of 7% when compared with 0% concentration channel. For 6% nano particles addition in all channels, on average both dual wavy channels showed the maximum improvement of 8% when compared with 0% concentration channel. Compared to the straight channel of equal concentration dual wavy channel showed maximum temperature drop of an average of 10 °C for wavy base and 9 °C for flat base channel at Re = 300. Dean vortices formation in the wavy channel enhances the heat transfer as a result circulating heat from the base of the microchannel, thus creating a cooling effect. Increase in nanoparticles concentration leads increase in the Nusselt number and pressure drop. Development of early counter rotating regular vortices in dual wavy channel helps in reduction of a base temperature. The formation of regular occurring vortices over the interval of wave curve help in convective heat transfer improvement and reduction of pressure drop. On the other hand, erratic flow in the wave increases pressure drop. TPF of a dual wavy channel for each concentration remained non-overlapping and maximum TPF of 2.2 is achieved for a wavy base dual wavy channel with 6% nano-particles concentration at Re = 600, whereas, flat base channel showed a TPF of 1.95 for 6% alumina concentration at Re = 600. Considering wavy microchannel a maximum TPF of 2.1 is observed for 3% alumina concentration at Re = 900.

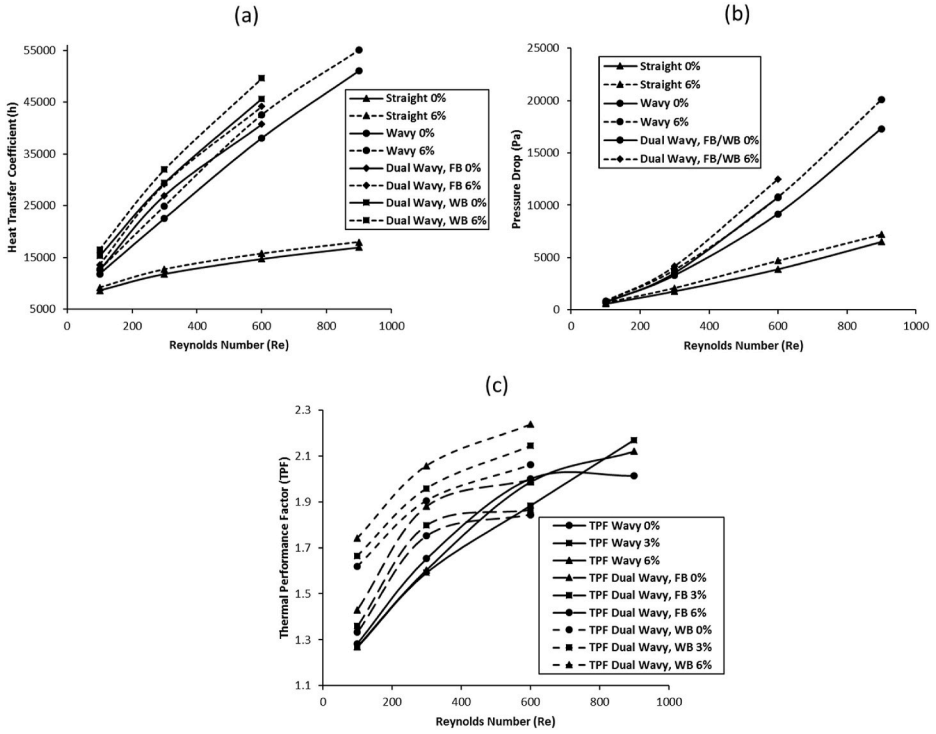

Fig. 11. Performance comparison of geometries based on parameters a) Heat transfer coefficient, b) Pressure drop, and c) Thermal Performance Factor (TPF).

Author statement

Muhammad Zia Ullah Khan: Conceptualization, Methodology, Software Bilal Akbar: Data curation, Writing – original draft preparation. Naveed Akram: Visualization, Investigation, Data curation, Writing – original draft. Md. Yamin Younis: Supervision.: Rumeel Ahmad Bhutta: Software, Validation.: Emad Uddin: Writing – review & editing; Muhammad Ahsan Jamil. Data curation, Writing – original draft preparation; Fausto Pedro García Márquez: Data curation, Writing – original draft preparation; Fahad Bin Zahid: Software, Validation

Declaration of competing interest

The authors declare that they have no known competing financial interests or personal relationships that could have appeared to influence the work reported in this paper.

References

[1] R. Law, A. Harvey, D. Reay, Opportunities for low-grade heat recovery in the UK food processing industry, Appl. Therm. Eng. 53 (2) (2013) 188–196.
[2] M.Z.U. Khan, et al., Investigation of heat transfer and pressure drop in microchannel heat sink using Al2O3 and ZrO2 nanofluids, Nanomaterials 10 (9) (2020) 1796.
[3] M.M. Thalib, et al., Comparative study of Tubular solar stills with phase change material and nano-enhanced phase change material, Energies 13 (15) (2020) 3989.
[4] S. Kumar, P.K. Singh, Effects of flow inlet angle on flow maldistribution and thermal performance of water cooled mini-channel heat sink, Int. J. Therm. Sci. 138 (2019) 504–511.
[5] X. Xiang, et al., A comparison between cooling performances of water-based and gallium-based micro-channel heat sinks with the same dimensions, Appl. Therm. Eng. 137 (2018) 1–10.
[6] M. Dhiman, et al., CFD analysis of greenhouse heating using flue gas and hot water heat sink pipe networks, Comput. Electron. Agric. 163 (2019), 104853.
[7] S. Deldar, M. Khoshvaght-Aliabadi, Evaluation of water-cooled heat sink with complex designs of groove for application in fusion energy management, Fusion Eng. Des. 140 (2019) 107–116.
[8] D.B. Tuckerman, R.F.W. Pease, High-performance heat sinking for VLSI, IEEE Electron. Device Lett. 2 (5) (1981) 126–129.
[9] P.-S. Lee, S.V. Garimella, Thermally developing flow and heat transfer in rectangular microchannels of different aspect ratios, Int. J. Heat Mass Tran. 49 (17–18) (2006) 3060–3067.
[10] M.K. Kang, et al., Analysis of laminar convective heat transfer in micro heat exchanger for stacked multi-chip module, Microsyst. Technol. 11 (11) (2005) 1176–1186.
[11] I. Hassan, P. Phutthavong, M. Abdelgawad, Microchannel heat sinks: an overview of the state-of-the-art, Microscale Thermophys. Eng. 8 (3) (2004) 183–205.
[12] S. Sindhu, B. Gireesha, D. Ganji, Simulation of Cu: γ− ALOOH/Water in a microchannel heat sink by dint of porous media approach, Case Studies Thermal Eng. 21 (2020), 100723.

[13] P. Xu, et al., Thermal characteristics of tree-shaped microchannel nets with/without loops, Int. J. Therm. Sci. 48 (11) (2009) 2139–2147.
[14] D. Heymann, D. Pence, V. Narayanan, Optimization of fractal-like branching microchannel heat sinks for single-phase flows, Int. J. Therm. Sci. 49 (8) (2010) 1383–1393.
[15] J.C. Kurnia, A.P. Sasmito, A.S. Mujumdar, Numerical investigation of laminar heat transfer performance of various cooling channel designs, Appl. Therm. Eng. 31 (6–7) (2011) 1293–1304.
[16] Y. Sui, P. Lee, C. Teo, An experimental study of flow friction and heat transfer in wavy microchannels with rectangular cross section, Int. J. Therm. Sci. 50 (12) (2011) 2473–2482.
[17] Y. Sui, et al., Fluid flow and heat transfer in wavy microchannels, Int. J. Heat Mass Tran. 53 (13–14) (2010) 2760–2772.
[18] M. Emam, M. Ahmed, Cooling concentrator photovoltaic systems using various configurations of phase-change material heat sinks, Energy Convers. Manag. 158 (2018) 298–314.
[19] M. Avci, M.Y. Yazici, An experimental study on effect of inclination angle on the performance of a PCM-based flat-type heat sink, Appl. Therm. Eng. 131 (2018) 806–814.
[20] X.-H. Yang, et al., Finned heat pipe assisted low melting point metal PCM heat sink against extremely high power thermal shock, Energy Convers. Manag. 160 (2018) 467–476.
[21] M. Zargartalebi, J. Azaiez, Heat transfer analysis of nanofluid based microchannel heat sink, Int. J. Heat Mass Tran. 127 (2018) 1233–1242.
[22] P. Naphon, L. Nakharintr, S. Wiriyasart, Continuous nanofluids jet impingement heat transfer and flow in a micro-channel heat sink, Int. J. Heat Mass Tran. 126 (2018) 924–932.
[23] L. Yang, K. Du, A comprehensive review on the natural, forced, and mixed convection of non-Newtonian fluids (nanofluids) inside different cavities, J. Therm. Anal. Calorim. (2019) 1–22.
[24] N. Tran, Y.-J. Chang, C.-C. Wang, Optimization of thermal performance of multi-nozzle trapezoidal microchannel heat sinks by using nanofluids of Al2O3 and TiO2, Int. J. Heat Mass Tran. 117 (2018) 787–798.
[25] S.U. Choi, J.A. Eastman, Argonne National Lab., IL (United States), Enhancing Thermal Conduct. Fluids Nanoparticles (1995). ANL/MSD/CP-84938CONF-951135-29.
[26] O. Yıldız, et al., Single phase flow of nanofluid including graphite and water in a microchannel, Heat Mass Tran. 56 (1) (2020) 1–24.
[27] L. Yang, et al., Numerical assessment of Ag-water nano-fluid flow in two new microchannel heatsinks: thermal performance and thermodynamic considerations, Int. Commun. Heat Mass Tran. 110 (2020), 104415.
[28] L. Yang, K. Du, Z. Zhang, Heat transfer and flow optimization of a novel sinusoidal minitube filled with non-Newtonian SiC/EG-water nanofluids, Int. J. Mech. Sci. 168 (2020), 105310.
[29] M. Fares, A.-M. Mohammad, A.-S. Mohammed, Heat transfer analysis of a shell and tube heat exchanger operated with graphene nanofluids, Case Studies Thermal Eng. 18 (2020), 100584.
[30] D.G. Subhedar, B.M. Ramani, A. Gupta, Experimental investigation of heat transfer potential of Al2O3/Water-Mono Ethylene Glycol nanofluids as a car radiator coolant, Case Studies Thermal Eng. 11 (2018) 26–34.
[31] M.S. Baba, A.S.R. Raju, M.B. Rao, Heat transfer enhancement and pressure drop of Fe3O4-water nanofluid in a double tube counter flow heat exchanger with internal longitudinal fins, Case Studies Thermal Eng. 12 (2018) 600–607.
[32] N. Akram, et al., Experimental investigations of the performance of a flat-plate solar collector using carbon and metal oxides based nanofluids, Energy (2021), 120452.
[33] A.H. Al-Waeli, et al., Evaluation of the electrical performance of a photovoltaic thermal system using nano-enhanced paraffin and nanofluids, Case Studies Thermal Eng. (2020), 100678.
[34] Q.A. Jawad, et al., Improve the performance of a solar air heater by adding aluminum chip, paraffin wax, and nano-SiC, Case Studies Thermal Eng. (2020), 100622.
[35] N. Akram, et al., An experimental investigation on the performance of a flat-plate solar collector using eco-friendly treated graphene nanoplatelets–water nanofluids, J. Therm. Anal. Calorim. 138 (1) (2019) 609–621.
[36] N. Akram, et al., A comprehensive review on nanofluid operated solar flat plate collectors, J. Therm. Anal. Calorim. 139 (2) (2019) 1–35.
[37] M.-J. Kao, et al., Producing aluminum-oxide brake nanofluids using plasma charging system, J. Chinese Soc. Mechanical Eng. 28 (2) (2007) 123–131.
[38] W. Ahmed, et al., Effect of ZnO-water based nanofluids from sonochemical synthesis method on heat transfer in a circular flow passage, Int. Commun. Heat Mass Tran. 114 (2020), 104591.
[39] W. Ahmed, et al., Experimental investigation of convective heat transfer growth on ZnO@ TiO 2/DW binary composites/hybrid nanofluids in a circular heat exchanger, J. Therm. Anal. Calorim. (2020) 1–20.
[40] M.H. Fard, M.N. Esfahany, M. Talaie, Numerical study of convective heat transfer of nanofluids in a circular tube two-phase model versus single-phase model, Int. Commun. Heat Mass Tran. 37 (1) (2010) 91–97.
[41] A. Akbarinia, R. Laur, Investigating the diameter of solid particles effects on a laminar nanofluid flow in a curved tube using a two phase approach, Int. J. Heat Fluid Flow 30 (4) (2009) 706–714.
[42] A. Mokmeli, M. Saffar-Avval, Prediction of nanofluid convective heat transfer using the dispersion model, Int. J. Therm. Sci. 49 (3) (2010) 471–478.
[43] A. Ebrahimi, et al., Heat transfer and entropy generation in a microchannel with longitudinal vortex generators using nanofluids, Energy 101 (2016) 190–201.
[44] U. Rea, et al., Laminar convective heat transfer and viscous pressure loss of alumina–water and zirconia–water nanofluids, Int. J. Heat Mass Tran. 52 (7–8) (2009) 2042–2048.
[45] F. Sadegh Moghanlou, et al., Experimental investigation of heat transfer and pressure drop in a minichannel heat sink using Al 2 O 3 and TiO 2–water nanofluids, J. Braz. Soc. Mech. Sci. Eng. 42 (2020) 1–11.
[46] A.N. Al-Shamani, et al., Enhancement heat transfer characteristics in the channel with Trapezoidal rib–groove using nanofluids, Case Studies in Thermal Eng. 5 (2015) 48–58.
[47] C. Ho, et al., Experimental study of cooling characteristics of water-based alumina nanofluid in a minichannel heat sink, Case Studies Thermal Eng. 14 (2019), 100418.
[48] H.M. Ammar, et al., Heat transfer comparative analysis: straight channel and dimple-protrusion overlapping with copper oxide nano-particles, in: 2021 4th International Conference on Energy Conservation and Efficiency (ICECE), IEEE, 2021.
[49] M.Z.U. Khan, et al., Investigation of heat transfer in dimple-protrusion micro-channel heat sinks using copper oxide nano-additives, Case Studies Thermal Eng. (2021), 101374.
[50] A.K. Santra, S. Sen, N. Chakraborty, Study of heat transfer due to laminar flow of copper–water nanofluid through two isothermally heated parallel plates, Int. J. Therm. Sci. 48 (2) (2009) 391–400.
[51] M. Rahman, et al., Numerical investigation of heat transfer enhancement of nanofluids in an inclined lid-driven triangular enclosure, Int. Commun. Heat Mass Tran. 38 (10) (2011) 1360–1367.
[52] H. Mohammed, P. Gunnasegaran, N. Shuaib, Numerical simulation of heat transfer enhancement in wavy microchannel heat sink, Int. Commun. Heat Mass Tran. 38 (1) (2011) 63–68.
[53] H. Mohammed, P. Gunnasegaran, N. Shuaib, Influence of channel shape on the thermal and hydraulic performance of microchannel heat sink, Int. Commun. Heat Mass Tran. 38 (4) (2011) 474–480.
[54] E.M. Abo-Zahhad, et al., Thermal management of high concentrator solar cell using new designs of stepwise varying width microchannel cooling scheme, Appl. Therm. Eng. 172 (2020), 115124.
[55] H.I. Elqady, et al., Concentrator photovoltaic thermal management using a new design of double-layer microchannel heat sink, Sol. Energy 220 (2021) 552–570.
[56] A.K. Jaiswal, P.S. Mahapatra, B.V. Prasad, Effect of microchannel on combined impingement and film cooling of a concave surface, Int. Commun. Heat Mass Tran. 126 (2021), 105441.

[57] Y. Huang, et al., Effects of wall cooling with microchannels on swirl combustor performance, Aero. Sci. Technol. 106 (2020), 106160.
[58] R. Avinash Kumar, et al., Numerical study of graphene-platinum hybrid nanofluid in microchannel for electronics cooling, Proc. IME C J. Mech. Eng. Sci. (2021), https://doi.org/10.1177/0954406220987261, 0954406220987261.
[59] M. Yang, et al., Experimental study on single-phase hybrid microchannel cooling using HFE-7100 for liquid-cooled chips, Int. J. Heat Mass Tran. 160 (2020), 120230.
[60] Y.A. Çengel, J.M. Cimbala, Fluid Mech.: Fundament. Applications, McGraw-hill higher education, 2010.
[61] A. Okhotin, A. Pushkarskii, V. Gorbachev, Thermophysical Properties of Semiconductors, Atom Publ. House, 1972. Moscow.
[62] A. Ebrahimi, E. Roohi, S. Kheradmand, Numerical study of liquid flow and heat transfer in rectangular microchannel with longitudinal vortex generators, Appl. Therm. Eng. 78 (2015) 576–583.
[63] T.L. Bergman, et al., Fundament. Heat Mass Trans, John wiley & sons New York, 2017.
[64] A.M. Sahar, et al., Single phase flow pressure drop and heat transfer in rectangular metallic microchannels, Appl. Therm. Eng. 93 (2016) 1324–1336.
[65] J.F. Price, Lagrangian and eulerian representations of fluid flow: Kinematics and the equations of motion, MIT OpenCourseWare, 2006, pp. 1–99.
[66] C. Hansel, Mapping of Pressure Losses Through Microchannels With Sweeping-Bends of Various Angle and Radii, 2008.
[67] C. Chen, et al., A study on fluid flow and heat transfer in rectangular microchannels with various longitudinal vortex generators, Int. J. Heat Mass Tran. 69 (2014) 203–214.